Title
Magnetization reversal in perpendicularly magnetized L10 FePd/FePt heterostructures

Journal
Journal of Applied Physics, 116(3)

ISSN
0021-8979

Authors
Ma, L
Gilbert, DA
Neu, V
et al.

Publication Date
2014-07-21

DOI
10.1063/1.4890936

Peer reviewed

Magnetization reversal in perpendicularly magnetized $L1_0$ FePd/FePt heterostructures

L. Ma,[1] D. A. Gilbert,[2] V. Neu,[3] R. Schäfer,[3,4] J. G. Zheng,[5] X. Q. Yan,[6] Z. Shi,[1] Kai Liu,[2] and S. M. Zhou[1,a)]

[1]*Shanghai Key Laboratory of Special Artificial Microstructure and Pohl Institute of Solid State Physics and School of Physics Science and Engineering, Tongji University, Shanghai 200092, China*
[2]*Department of Physics, University of California, Davis, California 95616, USA*
[3]*Leibniz Institute for Solid State and Materials Research IFW Dresden, Institute of Metallic Materials, Postfach 270116, 01171 Dresden, Germany*
[4]*Dresden University of Technology, Institute for Materials Science, 01062 Dresden, Germany*
[5]*The Laboratory for Electron and X-ray Instrumentation, Calit2, University of California, Irvine, California 92697, USA*
[6]*Nantong College, Jiangsu Open University, Nantong 226006, Jiangsu, China*

(Received 13 June 2014; accepted 4 July 2014; published online 21 July 2014)

The magnetization reversal process is investigated in perpendicular spring magnets of epitaxial $L1_0$ FePd/FePt (24 nm) thin films with varying FePd thickness. For thin FePd layers, the reversal is initiated by the nucleation of reversed bubble domains and is then mainly accomplished by the depinning and lateral movement of domain walls. For thick FePd layers, the magnetization reversal is predominantly governed by the nucleation process rather than wall motion, resulting in an increased density of bubble domains at more negative magnetic fields. The switching field is reduced significantly with increasing FePd thickness and exchange springs are formed locally due to a tilted magnetization in the FePd. These results arise from the interplay between differently strong perpendicular magnetic anisotropies in FePd and FePt and from layer dependent structural modifications, which is important for high density magnetic recording media. © *2014 AIP Publishing LLC*. [http://dx.doi.org/10.1063/1.4890936]

As one of the leading candidates for the next-generation magnetic recording technology, magnetic bilayers consisting of a high-anisotropy hard layer and low-anisotropy soft layer can provide a solution to the magnetic recording trilemma, i.e., the balance among writability, thermal stability, and signal to noise ratio, although they were initially proposed for permanent magnetic materials.[1,2] The magnetization reversal mechanism has been studied previously in various hard/soft bilayers or multilayers because the onset of the irreversible switching is crucial to magnetic device functionality,[2,3] and also indicative of the interlayer coupling and magnetic anisotropy of constituent layers.[4] For in-plane magnetized soft/hard bilayers with a thin soft layer, the magnetization in the two layers is reversed together due to the exchange coupling at the interface, i.e., in rigid mode.[5,6] For thick soft layers, the magnetization reversal process begins with reversible switching of the soft layer, and the switching field of the hard layer can be significantly reduced through exchange coupling with the soft layer, forming an exchange spring magnet.[5,7] It was previously suggested that also for orthogonally coupled hard and soft layers, e.g., Fe(in-plane)/$L1_0$-FePt(perpendicular), the switching field in the hard layer could be reduced.[8–12] The in-plane and orthogonally magnetized bilayers have distinct features in the magnetization reversal process. For the latter ones such as Fe/$L1_0$-FePt, the exchange spring may already exist at the remnant state for thick soft layers.[11,12] Recently, $[Co/Pt]_n$/$L1_0$-FePt and $L1_0$ CoPt-TiO_2/FePt-TiO_2 bilayers have been fabricated,[13–15] where the soft layer is also perpendicularly magnetized. This construction will not form the usual exchange spring structure, but can form domain walls which can freely propagate through the structure. Thus, this approach significantly reduces the reversal field but by a different mechanism from the previous in-plane and orthogonally coupled structures.

In this work, we have investigated the magnetization reversal mechanism in epitaxially grown $L1_0$ soft $Fe_{0.5}Pd_{0.5}$ (FePd)/hard $Fe_{0.5}Pt_{0.5}$(FePt) heterostructures. Since the perpendicular magnetic anisotropy (PMA) of 1×10^6 erg/cm^3 in the FePd is smaller than the demagnetization energy,[16] anisotropic properties of the present FePd/FePt heterostructures are different from those of orthogonally coupled bilayers[11,12] and perpendicularly magnetized bilayers.[13–15] For thin FePd samples, the magnetization reversal is mainly accomplished by depinning and lateral domain wall motion after the initial nucleation of reversed bubble domains. For thick FePd layers, the density of nucleation sites increases steadily at increasing reversal field, initiated by the stray field driven formation of magnetization swirls in the FePd film that expand into the FePt film. Due to the perpendicular moment orientation in the FePt layer in a certain field range, an exchange spring is expected, which however is laterally confined to the bubble/stripe domains, unlike in-plane exchange spring systems. The switching field is significantly reduced for thick FePd layers.

A series of $L1_0$ (top)FePd (thickness $t_s = 0$–31 nm)/(bottom) FePt (24 nm) bilayers were deposited on polished MgO (001) single crystal substrates by DC magnetron sputtering

a)Author to whom correspondence should be addressed. Electronic mail: shiming@tongji.edu.cn

from composite FePt and FePd targets. The targets were formed by putting small Pt and Pd pieces on two Fe targets, respectively. The base pressure of the deposition chamber was 1×10^{-5} Pa, and the working Ar pressure was 0.38 Pa. Before deposition, the substrates were desiccated and cleaned by heating them to 690 °C for 30 min. During deposition, the substrates were kept at this temperature. After deposition, the samples were annealed in-situ at 690 °C for 150 min. Structural properties and film thickness were determined by X-ray diffraction (XRD) and X-ray reflectivity using Cu Kα radiation, as well as transmission electron microscopy (TEM). The film surface roughness was characterized by atomic force microscopy (AFM). Domain structures were characterized by high resolution Kerr microscopy in the polar geometry.[17] Magnetic properties were measured by vibrating sample magnetometry, including detailed investigations of the magnetization reversal using the first-order reversal curve (FORC) technique.[18–20] All measurements were performed at room temperature.

Figure 1(a) shows the XRD patterns of the FePd (t_s)/FePt bilayers with different t_s. The presence of the FePd and FePt (001) diffraction peak at $2\theta = 24°$ indicates the establishment of tetragonal $L1_0$ ordering. Since the FePd and FePt layers have very similar c lattice parameters, the diffraction peaks

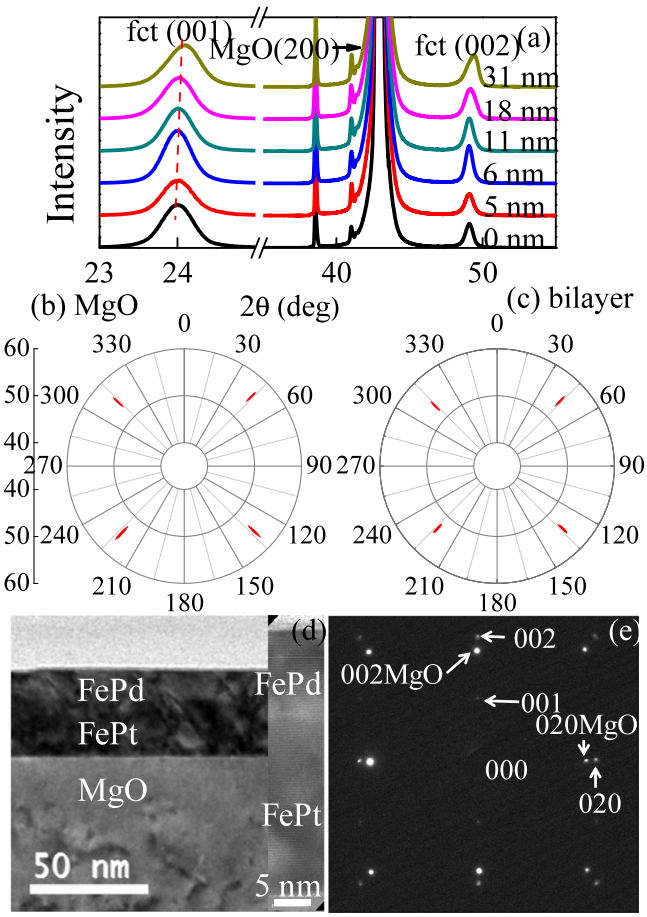

FIG. 1. XRD spectra of typical $L1_0$ FePd/FePt bilayers (a), the pole figures of MgO substrate (b) and film (c), and TEM image of a cross-sectional bilayer (d) and a selected area diffraction (e) from the sample with 11 nm FePd layer. The inset numbers in (a) refer to the FePd thickness. The inset in (d) refers to a zoomed-in image of the FePd/FePt bilayer.

are indistinguishable and thus cannot be used to determine the degree of ordering. In order to estimate the order parameter S of the constituent layers, FePt and FePd single layer films were prepared under the same conditions used for the FePt/FePd bilayers, and the S is calculated to be 0.8 using integrated intensities of the (001) and (002) peaks. The epitaxial growth was demonstrated by Φ and Ψ scans at $2\theta = 37.37°$ and 41.07° for the (111) reflection of MgO substrates and FePt/FePd films, as shown in Figs. 1(b) and 1(c), respectively. The same four-fold symmetry is found in both bilayers and MgO (001) substrates, indicating a good epitaxial growth of the films. The film quality was further examined by TEM. Figure 1(d) shows a typical bright field TEM micrograph of the cross-section of a FePd(11 nm)/FePt(24 nm) bilayer. Some defects (dislocations, twin boundaries and antiphase boundaries) were observed in the bilayer, but both FePd and FePt layers are single crystal with an epitaxial growth along the [001] direction, illustrated in the zoomed-in inset in Fig. 1(d). Figure 1(e) is a selected area electron diffraction (SAED) pattern from the bilayer and MgO substrate. There are two sets of SAED patterns associated with MgO and the bilayer, respectively. Again, the close lattice spacings make the FePd and FePt peaks indistinguishable. Because of the $L1_0$ ordering in the bilayer, the (001) diffraction spot shows up clearly in Fig. 1(e). The orientation relationship between the substrate and the bilayer is (001)bilayer// (001)MgO and [100]bilayer//[100]MgO. Forming a lattice image with a small objective aperture including three spots ± (001) bilayer and 000, the lattice fringes of (001) planes of FePd and FePt layers can be revealed, as shown in the inset of Fig. 1(d). The interface between FePd and FePt can be readily seen. FePd and FePt layers were further confirmed by Z-contrast scanning transmission electron microscope (STEM) and Energy Dispersive Spectroscopy (EDS) composition analysis. The film surface roughness has been characterized by AFM, and the root mean square (RMS) surface roughness is 0.48, 1.18, and 1.28 (nm) for $t_s = 5$, 11, and 31 (nm), respectively. Apparently, the surface roughness increases for thicker FePd layers.

Figures 2(a)–2(c) show hysteresis loops of typical FePd/FePt bilayers ($t_s = 5$, 11, 31 nm). For thin FePd samples, such as $t_s = 5$ and 11 nm, a strong PMA is indicated by the square out-of-plane hysteresis loops and slanted in-plane ones, as shown in Figs. 2(a) and 2(b). The out-of-plane loop becomes pinched for $t_s = 31$ nm, and the film normal is no longer the direction of easy axis. This is demonstrated directly by plotting the out-of-plane coercivity H_C and the domain nucleation field, as shown in Figs. 2(d) and 2(e), respectively. Both these quantities decrease in magnitude for increasing FePd layer thickness, and the nucleation field actually changes from negative to positive. The trend lines show that H_C decreases sharply up to $t_s = 8$ nm and then gradually saturates at higher t_s, whereas the nucleation field changes continuously for all thicknesses.

In order to reveal the magnetization reversal mechanisms, the magnetic hysteresis loops were measured when the angle (θ_H) between H and the film normal direction changes from 0° to 90°. Figure 2(f) shows that for thin (5 nm) FePd samples, H_C initially increases as $1/\cos\theta_H$,

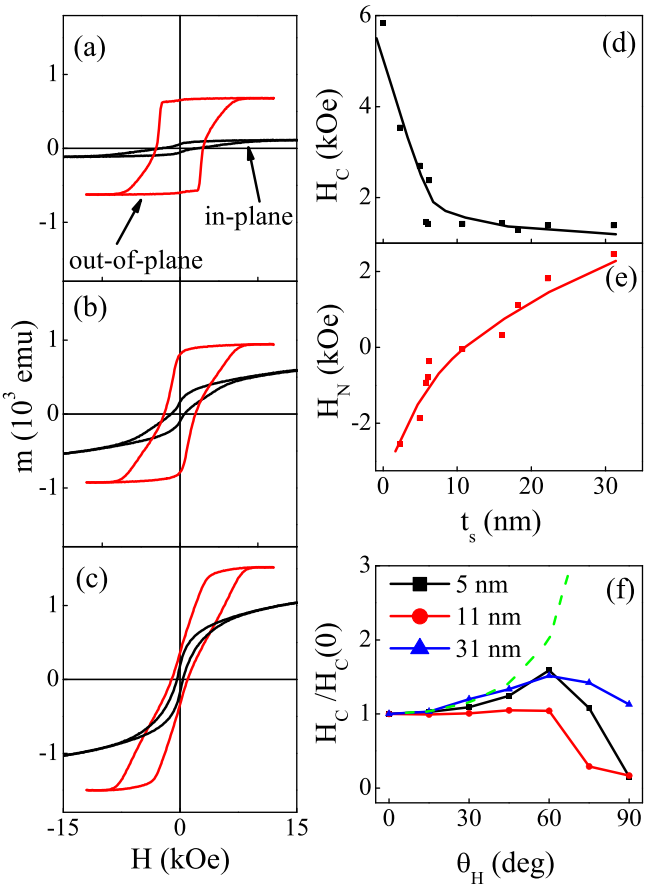

FIG. 2. Out-of-plane and in-plane hysteresis loops of FePd/FePt bilayers with $t_s = 5$ nm (a), 11 nm (b), and 31 nm (c), the t_s dependences of the out-of-plane H_C (d) and nucleation field (e), and the angular dependence of H_C(f), where θ_H refers to the angle between H and the film normal direction. In (a)–(c), the sampling area is 0.25 cm^2. In (f), the inset numbers refer to the FePd layer thickness t_s and the dashed line corresponds to the mode of the domain wall motion depinning.

shown by the dashed line, and then decreases for θ_H larger than a critical angle, obeying a modified Kondorsky model.[14,21] For $t_s = 11$ nm, the H_C has little change at small θ_H and decreases with further increasing θ_H. Since for the bilayer with $t_s = 31$ nm the film normal is no longer the direction of preferred magnetization orientation, the magnetization reversal mechanism should be different from that of $t_s = 5$ nm despite their similar angular dependences of the H_C. Apparently, all samples reverse by an incoherent reversal process.[22]

The Kerr images in Figs. 3(a)–3(i) show static domain structure with decreasing H after positive saturation, where the white and black contrast corresponds to out-of-plane up and down magnetizations, respectively. Since the magneto-optical Kerr effect in FePd is much smaller than that in FePt,[23,24] the Kerr contrast in the double films is mainly coming from the hard FePt layer. In a comparative experiment (not shown), no Kerr contrast could be observed for FePd single layer films and $t_s = 31$ nm bilayers with FePd on top. As a reference, in a single 16 nm thick $L1_0$ FePt film, (Figs. 3(a)–3(c)) the reversal proceeds mainly by domain wall motion after bubble domain nucleation at selected locations, resulting in a complex maze-like domain pattern during reversal. This propagation of nucleated domains occurs abruptly [over 0.27 kOe as shown in Figs. 3(a)–3(c)], similar to that seen in other PMA systems,[18] and large areas of several square micrometers are immediately filled with oppositely magnetized stripe domains. In the FePd/FePt bilayers, the reversal process is significantly different: As the applied field becomes more negative, the density of bubble domains increases steadily [over 1 kOe, as shown in Figs. 3(d)–3(f) and 3(g)–3(i)] before they expand into stripe domains around the coercive field. This is true for $t_s = 5$ nm (Figs. 3(d)–3(f)) and even more pronounced for the sample with $t_s = 11$ nm (Figs. 3(g)–3(i)).

In order to further analyze details of the magnetization reversal process, the FORC technique was applied as follows:[18–20] After saturation, the magnetic field was first swept from positive saturation to a reversal field, H_R. The magnetization was then measured as the applied field, H_a, starting at $H_a = H_R$, was increased back towards positive saturation. This process was repeated with decreasing values of H_R until negative saturation was reached, thus collecting a family of FORCs. Here, neighboring FORCs are equally spaced in H_R. The FORC distribution $\rho(H_R, H_a)$ is determined by applying a mixed second order derivative to the magnetization.[25,26] Thus, one has the FORC distribution $\rho = 0$ for a reversible process and $\rho \neq 0$ for an irreversible one.

Families of FORCs for $t_s = 5$ nm, 11 nm, and 31 nm are shown in Figs. 4(a)–4(c), and the corresponding FORC distributions are shown in Figs. 4(d)–4(f), respectively. Four reference reversal fields are marked on the FORCs and the FORC distributions. A three-stage reversal process is clearly seen in all samples. First, the FORC distribution exhibits a horizontal ridge (boxed area a_1, between lines 1 & 2), due to the nucleation and growth of reversed domains[18] (as shown in Figs. 3(d)–3(f)). For example, for $t_s = 5$ nm, the major loop magnetization drops precipitously between points 1 and 2 in Fig. 4(a), corresponding to the propagation of reversed domains in this field range. The slope of the successive FORCs originating in this field range continues to increase when $H_a > 0$, as highlighted by the box a_2, leading to the FORC ridge shown in box a_1 of Fig. 4(d).[20] Second, between lines 2 and 3, the shallow FORC distribution indicates largely reversible expansion/contraction of domains. Finally, a negative/positive pair of peaks (regions b_1 and c_1, respectively, between lines 3 and 4) indicate that along this group of FORC's, residual domains are being annihilated as reversal field H_R approaches negative saturation, and new domains are being re-nucleated when the applied field H_a increases. These are observed directly in the family of FORC's: the slope of the magnetization decreases with successively more negative H_R ($\rho \leq 0$) in the area b_2 and increases in the area c_2 ($\rho \geq 0$). With increasing t_s, the FORC features are tilted clockwise and stretched diagonally in the H_a–H_R coordinates [Figs. 4(d)–4(f)]: the horizontal ridge (boxed area a_1) moves towards more positive (H_a, H_R). For $t_s = 5$ nm, 11 nm, and 31 nm, the center of the FORC ridge shifts to (4.0 kOe,−2.6 kOe), (4.9 kOe, −1.0 kOe), and (6.1 kOe, 2.1 kOe), respectively. Meanwhile, the negative/positive pair of peaks (regions b_1 and c_1) shifts towards more negative H_a for large t_s, centering at $H_a = 2.7$ kOe, 0.90 kOe, and −2.2 kOe, respectively, for the three t_s's. The tilting is a

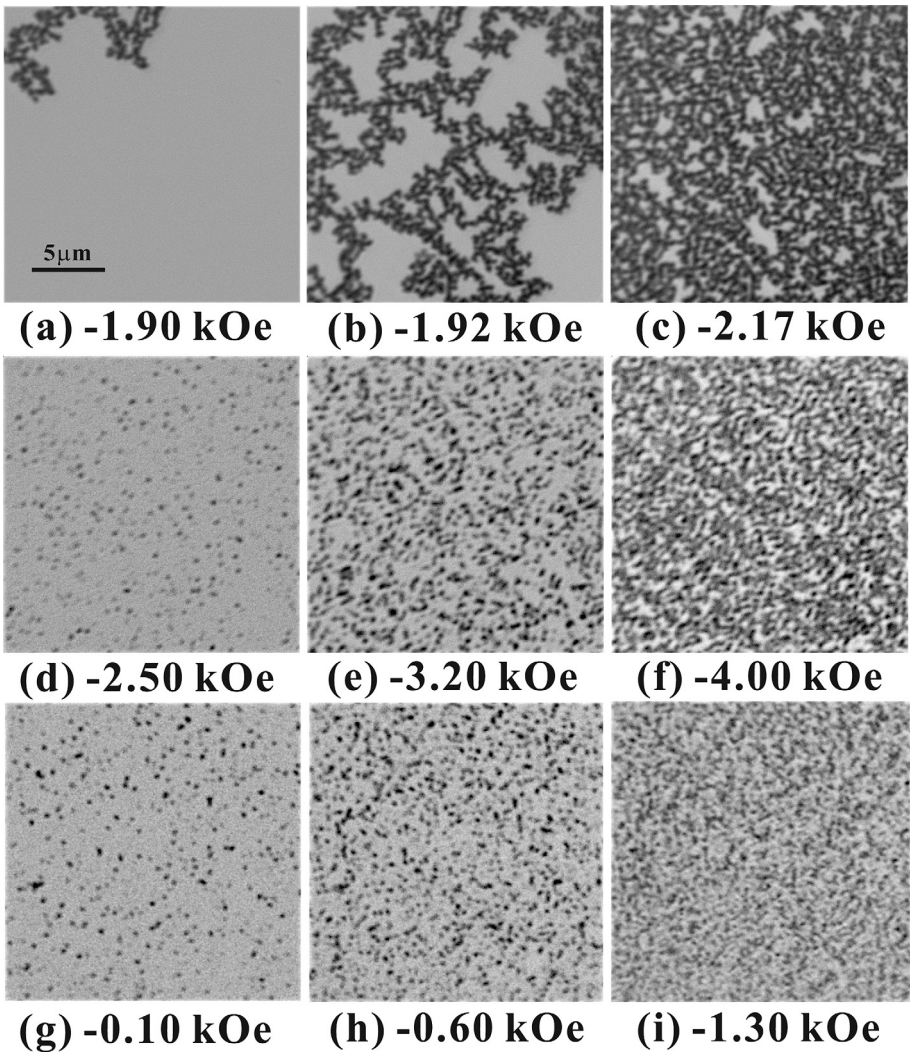

FIG. 3. Domain images of $L1_0$ FePt single film (a–c), FePd (5 nm)/FePt bilayer (d–f), and FePd (11 nm)/FePt bilayer (g–i), observed by Kerr microscopy at the indicated magnetic field values.

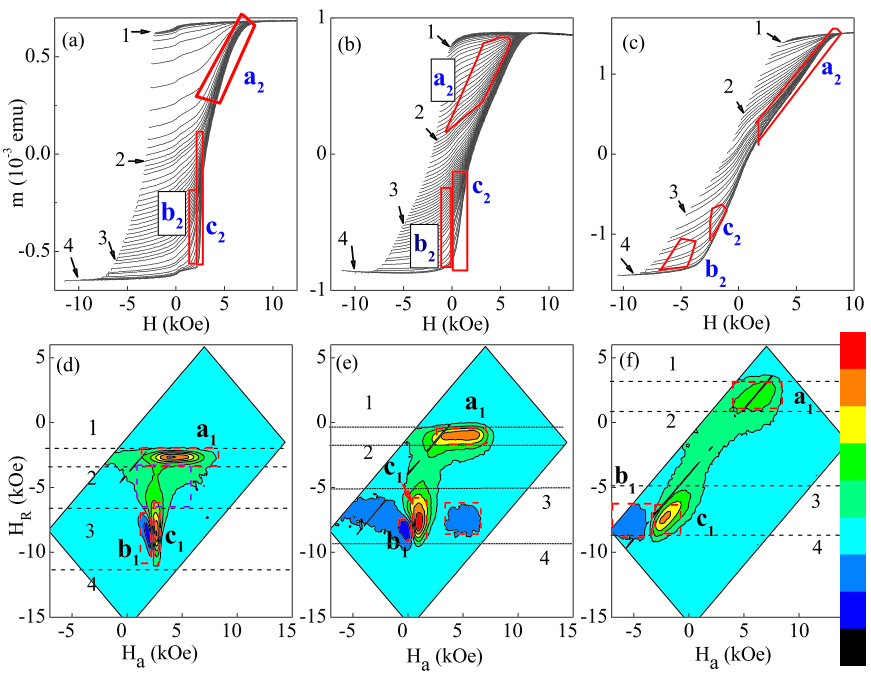

FIG. 4. Family of the FORCs (a)–(c) and the corresponding FORC distributions (d)–(f) for FePd/FePt bilayers with $t_s = 5$ nm (a) and (d), 11 nm (b) and (e), and 31 nm (c) and (f), respectively. For each sample, the a_1, b_1, and c_1 areas in the bottom contour correspond to the a_2, b_2, and c_2 areas in the upper FORC panel.

direct consequence of the increasing demagnetization effect in the thicker films, which also manifests in the more slanted hysteresis loop shown in Fig. 4(c). Moreover, the FORC ridge a_1 in the $t_s = 31$ nm sample [Fig. 4(c)] has largely collapsed, indicating much reduced irreversible switching during stage 1 of the reversal. This is consistent with the effects of graded magnetic anisotropy along the film depth and higher disorders, as seen in Co/Pd and Co/Pt systems.[27,28,31]

The significant change of the magnetization reversal mode by adding an FePd film on top of an FePt layer can be attributed to the interplay between weak perpendicular anisotropy, structural inhomogeneities and demagnetization energy. In pure FePt films (Figs. 3(a)–3(c)), the reversal proceeds mainly by domain wall propagation laterally across the film: at select locations ("week points"), bubble domains are first nucleated by reversing the field after positive saturation, which then branch out and coalesce into stripe domains at more negative fields. These reversed stripe domains propagate abruptly, occupying large areas of several square micrometers. These irregular stripe domains form a complex non-equilibrium pattern that is determined by the pinning energy landscape. For bilayers, the surface roughness is larger than that of the $L1_0$ FePt single layer films, and it increases with increasing t_s, as shown in the AFM results discussed earlier. At the same time, the additional FePd film adds further degrees of freedom for domain nucleation: whereas, in FePt single layers, the magnetization will rigidly follow the perpendicular easy axis for any domain state due to a quality factor $K_U/2\pi M_S^2 \gg 1$; in bilayers, there will be some (demagnetizing energy-driven) spin canting towards the surface in the FePd film when decreasing the field from saturation, which is due to a quality factor around 0.5 for FePd.[17] Together with the surface roughness, this canting favors the local nucleation of reversed domains in the FePd that extend into the FePt film during reversal. The roughness-induced pinning prevents unhindered expansion of labyrinth domains.[28,31] The reversal process in the thicker bilayers is thus dominated by nucleation, as demonstrated by the steady increase of the reversed bubble domains shown in Figs. 3(d)–3(i)), and the collapsed FORC feature a_1 in the thicker film (Fig. 4(f)). The exchange spring is expected to form locally in bubbles and vertically expands into the FePt layer at more negative field due to the dominant role of the demagnetization energy.[29,30] In contrast, for thin FePd samples, the FePd moments are strongly exchange coupled to the perpendicular FePt; the reversal process starts with nucleation of reversed domains throughout the entire bilayer depth, followed by irreversible lateral domain wall motion as demonstrated by both the bubble domain structure (Fig. 3(d)) and the FORC distribution (Fig. 4(d)) that are similar to those for the Co/Pt and Co/Pd multilayers.[18,30–32]

In summary, we have prepared epitaxial $L1_0$ FePd/FePt (24 nm) heterostructures on MgO(001) substrates and studied the evolution of the magnetization reversal mechanism with the FePd layer thickness by FORC and Kerr microscopy. For thin FePd samples, magnetic moments in both layers are strongly coupled together and remain perpendicular to the films; the magnetization reversal process is initialized by nucleation of reversed domains and mainly accomplished by irreversible domain wall motion. For thick FePd layers, the magnetization reversal is realized through local nucleation of reversed domains, where exchange springs are formed along the depth of the FePd/FePt films. The different reversal behaviors can be attributed to the combined effects of demagnetization energy, interfacial exchange coupling and disorders.

This work was supported by the National Science Foundation of China Grant Nos.11374227, 51331004, 51171129, and 51201114, Shanghai Nanotechnology Program Center (No. 0252 nm004), Shanghai Municipal Science and Technology Committee (13XD1403700 and 13520722700). Work at UCD was supported by the US NSF (DMR-1008791). TEM and FIB work was performed at the Laboratory for Electron and X-ray Instrumentation (LEXI) at UC Irvine, using instrumentation funded in part by the National Science Foundation Center for Chemistry at the Space-Time Limit (CHE-082913). Thanks also to A. Brunner (IFW) for assisting in Kerr microscopy.

[1]E. F. Kneller, IEEE Trans. Magn. **27**, 3588 (1991).
[2]R. Skomski, Phys. Rev. B **48**, 15812 (1993).
[3]Y. Suzuki, R. B. van Dover, E. M. Gyorgy, J. M. Phillips, and R. J. Felder, Phys. Rev. B **53**, 14016 (1996).
[4]F. García-Sánchez, O. Chubykalo-Fesenko, O. Mryasov, P. Asselin, and R. W. Chantrell, J. Appl. Phys. **103**, 07F505 (2008).
[5]E. E. Fullerton, J. S. Jiang, M. Grimsditch, C. H. Sowers, and S. D. Bader, Phys. Rev. B **58**, 12193 (1998).
[6]D. Chumakov, R. Schäfer, D. Elefant, D. Eckert, L. Schultz, S. S. Yan, and J. A. Barnard, Phys. Rev. B **66**, 134409 (2002).
[7]S. Sawatzki, R. Heller, C. Mickel, M. Seifert, L. Schultz, and V. Neu, J. Appl. Phys. **109**, 123922 (2011).
[8]J. P. Wang, W. K. Shen, J. M. Bai, R. Victora, J. Judy, and W. L. Song, Appl. Phys. Lett. **86**, 142504 (2005).
[9]R. H. Victora and X. Shen, IEEE Trans. Magn. **41**, 537 (2005).
[10]D. Suess, T. Schrefl, S. Fähler, M. Kirschner, G. Hrkac, F. Dorfbauer, and J. Fidler, Appl. Phys. Lett. **87**, 012504 (2005).
[11]G. Asti, M. Ghidini, R. Pellicelli, C. Pernechele, M. Solzi, F. Albertini, F. Casoli, S. Fabbrici, and L. Pareti, Phys. Rev. B **73**, 094406 (2006).
[12]J. L. Tsai, H. T. Tzeng, and G. B. Lin, Appl. Phys. Lett. **96**, 032505 (2010).
[13]D. Makarov, J. Lee, C. Brombacher, C. Schubert, M. Fuger, D. Suess, J. Fidler, and M. Albrecht, Appl. Phys. Lett. **96**, 062501 (2010).
[14]H. H. Guo, J. L. Liao, B. Ma, Z. Z. Zhang, Q. Y. Jin, H. Wang, and J. P. Wang, Appl. Phys. Lett. **100**, 142406 (2012).
[15]K. K. M. Pandey, J. S. Chen, and G. M. Chow, IEEE Trans. Magn. **46**, 1955 (2010).
[16]P. He, X. Ma, J. W. Zhang, H. B. Zhao, G. Lupke, Z. Shi, and S. M. Zhou, Phys. Rev. Lett. **110**, 077203 (2013).
[17]A. Hubert and R. Schäfer, *Magnetic Domains: The Analysis of Magnetic Microstructures* (Springer-Verlag, Berlin, 1998).
[18]J. E. Davies, O. Hellwig, E. E. Fullerton, G. Denbeaux, J. B. Kortright, and K. Liu, Phys. Rev. B **70**, 224434 (2004).
[19]R. K. Dumas, K. Liu, C. P. Li, I. V. Roshchin, and I. K. Schuller, Appl. Phys. Lett. **91**, 202501 (2007).
[20]D. A. Gilbert, G. T. Zimanyi, R. K. Dumas, M. Winklhofer, A. Gomez, N. Eibagi, J. L. Vicent, and K. Liu, Sci. Rep. **4**, 4204 (2014).
[21]E. Kondorsky, J. Phys. (Moscow) **2**, 161 (1940).
[22]P. Pawlik, J. J. Wäysocki, W. Kaszuwara, and M. Leonowicz, J. Magn. Magn. Mater. **242–245**, 1344 (2002).
[23]G. Armelles, D. Weller, B. Rellinghaus, R. F. C. Farrow, M. F. Toney, P. Caro, A. Cebollada, and M. I. Alonso, IEEE Trans. Magn. **33**, 3220 (1997).
[24]L. Ma, J. Hu, M. Costa, Z. Shi, J. Li, X. G. Xu, Y. Jiang, G. Y. Guo, R. Q. Wu, and S. M. Zhou, J. Appl. Phys. **115**, 183903 (2014).
[25]H. Wilde and H. Girke, Z. Angew. Phys. **11**, 339 (1959).

[26]C. Pike, Phys. Rev. B **68**, 104424 (2003).
[27]B. J. Kirby, J. E. Davies, K. Liu, S. M. Watson, G. T. Zimanyi, R. D. Shull, P. A. Kienzle, and J. A. Borchers, Phys. Rev. B **81**, 100405 (2010).
[28]M. Pierce, C. Buechler, L. Sorensen, S. Kevan, E. Jagla, J. Deutsch, T. Mai, O. Narayan, J. Davies, K. Liu, G. Zimanyi, H. Katzgraber, O. Hellwig, E. Fullerton, P. Fischer, and J. Kortright, Phys. Rev. B **75**, 144406 (2007).
[29]J. E. Davies, O. Hellwig, E. E. Fullerton, J. S. Jiang, S. D. Bader, G. T. Zimanyi, and K. Liu, Appl. Phys. Lett. **86**, 262503 (2005).
[30]D. Roy, K. V. Sreenivasulu, and P. S. A. Kumar, Appl. Phys. Lett. **103**, 222406 (2013).
[31]P. K. Greene, B. J. Kirby, J. W. Lau, J. A. Borchers, M. R. Fitzsimmons, and K. Liu, Appl. Phys. Lett. **104**, 152401 (2014).
[32]J. E. Davies, O. Hellwig, E. E. Fullerton, and K. Liu, Phys. Rev. B **77**, 014421 (2008).